Journal of Power Sources 237 (2013) 104–111

Contents lists available at SciVerse ScienceDirect

Journal of Power Sources

journal homepage: www.elsevier.com/locate/jpowsour

N-Alkyl-*N*-methylpyrrolidinium difluoro(oxalato)borate ionic liquids: Physical/electrochemical properties and Al corrosion

Joshua L. Allen [a,c], Dennis W. McOwen [a], Samuel A. Delp [a], Eric T. Fox [a], James S. Dickmann [a], Sang-Don Han [a], Zin-Bin Zhou [b], T. Richard Jow [c], Wesley A. Henderson [a,*]

[a] *Ionic Liquids & Electrolytes for Energy Technologies (ILEET) Laboratory, Department of Chemical & Biomolecular Engineering, North Carolina State University, Raleigh, NC 27695, USA*
[b] *School of Chemistry and Chemical Engineering, Huazhong University of Science and Technology, Wuhan 430074, China*
[c] *U.S. Army Research Laboratory, Adelphi, MD 20783, USA*

HIGHLIGHTS

- *N*-Alkyl-*N*-methylpyrrolidinium difluoro(oxalato)borate ILs have been synthesized.
- ILs are liquid at room temperature and have high thermal stabilities.
- ILs display high oxidative stability on Pt.
- ILs reversibly plate Li/Li^+ when mixed with common lithium salts.
- Corrosion of Al is negligible, even in IL–LiTFSI and IL–LiFSI mixtures.

ARTICLE INFO

Article history:
Received 5 November 2012
Received in revised form
8 January 2013
Accepted 26 February 2013
Available online 14 March 2013

Keywords:
Lithium-ion battery
LiDFOB
Electrolyte
Al corrosion
Ionic liquid

ABSTRACT

The synthesis and physical properties of difluoro(oxalato)borate ($DFOB^-$)-based ionic liquids (ILs) are reported with *N*-alkyl-*N*-methylpyrrolidinium ($PY_{1R}{}^+$) cations with butyl, pentyl and hexyl alkyl chains. The $PY_{14}DFOB$ and $PY_{16}DFOB$ salts have a melting point (T_m) of −5 °C and 31 °C, respectively, whereas the $PY_{15}DFOB$ salt does not crystallize. Instead, this salt has a glass transition temperature (T_g) of −74 °C. Electrolytes composed of these ILs are noncorrosive toward Al when mixed with LiTFSI and LiFSI, as well as with $LiPF_6$ or LiDFOB. The exceptional oxidative stability of these ILs suggests that they may be suitable for battery electrolyte applications.

1. Introduction

As Li-ion batteries are used in more demanding applications, the need for safer, more electrochemically/thermally stable, and more conductive electrolytes grows tremendously. This is especially true for new cell chemistries with high-voltage cathodes and/or alloy anodes. In particular, electrolytes are often considered a bottleneck in the development of the high-voltage cathode materials, as the current state-of-the-art electrolyte used in commercial Li-ion batteries, with mixed carbonate solvents and $LiPF_6$, does not enable stable long-term cycling of cells with such cathodes, especially at elevated temperatures. The principal means of addressing this challenge thus far has been through the use of electrolyte additives [1–8]. One such additive that has gained significant attention is lithium difluoro(oxalato)borate with the $DFOB^-$ anion:

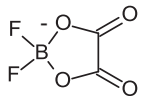

LiDFOB has been shown to stabilize various cathode materials, including (but not limited to) $LiCoPO_4$, $LiMn_2O_4$, $LiFePO_4$ and $Li_{1.1}[Mn_{1/3}Ni_{1/3}Co_{1/3}]_{0.9}O_2$ [7–11], yielding an improved performance when used as both a primary electrolyte salt (replacing $LiPF_6$) and in low (additive) concentrations (with $LiPF_6$). LiDFOB

* Corresponding author.
E-mail address: whender@ncsu.edu (W.A. Henderson).

0378-7753/$ – see front matter © 2013 Elsevier B.V. All rights reserved.
http://dx.doi.org/10.1016/j.jpowsour.2013.02.086

possesses the intrinsic ability to form an SEI layer on graphite anodes, even in high concentrations of propylene carbonate (PC), a solvent known to exfoliate graphene layers [11–14]. Furthermore, LiDFOB has also been shown to passivate the aluminum (Al) current collector, protecting it from corrosion [15,16]. Only a trace amount (i.e., 0.5–2.0 wt%) of an additive, such as LiDFOB, is generally used as a sacrificial agent to preferentially react on the electrode surface(s) within the first few cycles, producing a stabilizing interfacial layer(s). The additives thus do little to influence the electrolyte volatility, flammability and bulk electrolyte stability (should the passivation layer become disrupted).

Despite the improved performance of the industry-standard electrolyte with additives, significant attention has recently shifted to ionic liquids (ILs) as a viable alternative to traditional carbonate-based electrolytes. ILs possess many favorable properties including low volatility, low flammability, high electrochemical stability window, etc. [17–19]. However, Li-ion batteries that utilize IL-based electrolytes (without additives) suffer from poor charge–discharge performance due to the lack of SEI formation and thus increased irreversible capacity loss when cycled with a graphitic anode (due to the intercalation of the organic cations) [20–23]. Therefore, IL-based electrolytes require additives (perhaps in high concentration), such as lithium bis(fluorosulfonyl)imide ($LiN(SO_2F)_2$ or LiFSI) or FSI^--based ILs, to form a suitable SEI layer [22–25]. It may be desirable, however, to utilize ILs containing other anions, such as the $DFOB^-$ anion, to optimize properties for specific cell designs and applications. Thus far, 1-alkyl-3-methylimidazolium difluoro(oxalato) borate ($C_R$mimDFOB) ILs have been synthesized via a bidentate trimethylsilyl oxalate reaction with $C_R$mimBF_4 ILs [26]. ILs with these cations, however, are expected to display a significantly lower degree of stability toward oxidation and reduction than those with *N*-alkyl-*N*-methylpiperidinium (PI_{1R}^+) and *N*-alkyl-*N*-methylpyrrolidinium (PY_{1R}^+) cations [27,28].

The synthesis of *N*-alkyl-*N*-methylpyrrolidinium difluoro(oxalato)borate (PY_{1R}DFOB) ILs using a different (metathesis) procedure is reported here. The thermal properties of these ILs have been investigated, as well as their oxidation/reduction stability limits. Additionally, the Al corrosion properties of these ILs were tested with common lithium salts, including LiFSI and lithium bis(trifluoromethanesulfonyl)imide ($LiN(SO_2CF_3)_2$ or LiTFSI)—both of which are highly corrosive toward Al when used with carbonate solvents at higher potentials. These ILs show promise as battery electrolyte materials, as they combine the exceptional thermal stability and nonvolatility properties of many ILs with the graphite SEI forming and cathode stabilization properties of the $DFOB^-$ anion and the increased oxidative/reductive properties of (PY_{1R}^+) cations.

2. Experimental

2.1. Materials

Sodium oxalate (Sigma–Aldrich, ≥99%) was dried at 105 °C for 48 h, while boron trifluoride diethyl etherate (Sigma–Aldrich, ≥46.5% BF_3 basis), 1-methylpyrrolidine (Sigma–Aldrich, ≥98.0%) and bromoalkanes (Sigma–Aldrich: 1-bromobutane 99%, 1-bromopentane 99%, 1-bromohexane 98%) were used as-received. Diethyl ether (Et_2O, anhydrous, Sigma–Aldrich, ≥99.0%), acetonitrile (AN, anhydrous, Sigma–Aldrich, 99.8%), ethyl acetate (EA, anhydrous, Sigma–Aldrich, 99.8%), ethylene carbonate (EC, Sigma–Aldrich, 99%, <0.005% H_2O) and dimethyl carbonate (DMC, Sigma–Aldrich, ≥99%, <0.002% H_2O) were used as-received. Ethyl methyl carbonate (EMC, Ferro Corp., electrolyte grade) was dried over 3 Å molecular sieves for 1 week. The final water content of each solvent was verified to be negligible (<20 ppm) using a Mettler Toledo DL39 Karl Fischer coulometer. LiTFSI was purchased from 3 M and dried under high vacuum at 120 °C for 24 h prior to use. LiFSI (gratis, Suzhou Fluolyte Company, >99.5%) was used as-received. LiDFOB was synthesized as previously reported (≥99.9%) [29]. $LiPF_6$ and $LiBF_4$ (Novolyte, electrolyte-grade) were used as-received. Lithium bis(oxalato)borate (LiBOB, gratis, Chemetal) was purified by extraction/recrystallization in AN and then dried at 105 °C for 24 h prior to use. $LiBF_4$ and LiBOB were used only for the peak identification and detection limit determination for the ^{11}B-NMR measurements. Al electrodes were provided gratis from Argonne National Laboratory and represent the standard foil used as a current collector in state-of-the-art cathode fabrication. The materials were stored in sealed containers in a Vacuum Atmospheres glovebox with a N_2 atmosphere (<5 ppm O_2 and <1 ppm H_2O).

2.2. Synthesis/purification

2.2.1. Synthesis of NaDFOB

101.29 g (0.756 mol) of sodium oxalate was reacted with 109.78 g (0.773 mol) of boron trifluoride diethyl etherate in Et_2O. The slurry was stirred at 80 °C in a sealed container and allowed to react for 24 h. The excess BF_3 and Et_2O were then removed via vacuum filtration. The resulting sodium difluoro(oxalato)borate (NaDFOB) was extracted with AN and filtered to remove the unreacted sodium oxalate and NaF byproduct. The solution was concentrated, recrystallized (as an $(AN)_2$:NaDFOB solvate) and dried at 105 °C for 24 h to yield a highly pure NaDFOB powder. The crystal structure of the solvate, obtained from the recrystallized solids, has been previously reported [30].

2.2.2. Synthesis of $PY_{1R}Br$

N-Alkyl-*N*-methylpyrrolidinium bromide ($PY_{1R}Br$) salts were prepared by combining 1-methylpyrrolidine with an equimolar amount of the appropriate bromoalkane in EA. Upon stirring overnight at 60 °C, the previously homogeneous solutions formed slurries, confirming that reactions occurred. The resulting solid $PY_{1R}Br$ salts were filtered with a fine-frit glass filter and rinsed with excess amounts of EA. The recovered salts were then dried at 90 °C for 24 h and stored in sealed containers in the glovebox.

2.2.3. Synthesis of $PY_{1R}TFSI$ and $PY_{1R}DFOB$ ILs

$PY_{14}TFSI$ was synthesized as previously reported [31]. *N*-Alkyl-*N*-methylpyrrolidinium difluoro(oxalato)borate ($PY_{1R}DFOB$) ILs were synthesized by reacting NaDFOB with the appropriate $PY_{1R}Br$ salt (0.95:1.00 ratio), each dissolved in AN. The $PY_{1R}Br$ was used in excess such that the rinse solution could be monitored with silver nitrate (to ensure $PY_{1R}Br$ was fully removed). Upon adding the NaDFOB solutions to the $PY_{1R}Br$ solutions, a precipitate (i.e., NaBr) was instantly noted. The NaBr byproduct was filtered off. The resulting ILs (once the AN was removed from the filtrate via rotoevaporation) were then purified using the same procedure as for $PY_{14}TFSI$ [31]. The Br content was also measured via elemental analysis to confirm the absence of Br^- anion contamination in the ILs (see Supplementary data). The resulting ILs were vacuum dried at 60 °C for 48 h and stored in hermetically-sealed containers in the glovebox.

2.3. Thermal measurements

TGA measurements were performed using a TA Instruments Q5000 thermogravimetric analyzer. Each IL was heated at a rate of 10 °C min^{-1} from 25 °C to 150 °C (to remove residual moisture absorbed during sample loading), equilibrated for 90 min, cooled to 25 °C, and heated at a rate of 5 °C min^{-1} to 550 °C. The TGA furnace

was maintained under N_2 gas during all of the measurements. DSC analysis was performed using a TA Instruments Q2000 differential scanning calorimeter. The instrument was calibrated with cyclohexane (solid-solid phase transition at −87.06 °C, melting transition (T_m) at 6.54 °C) and indium (T_m at 156.60 °C). Each IL was hermetically sealed in Al pans in the glovebox. The ILs were cooled to −150 °C and heated at a rate of 5 °C min^{-1} to 200 °C. The samples were cycled/annealed multiple times below/above their glass transition temperature (T_g) until crystallization was observed. If crystallization was not achieved after five cycles, it was assumed that the sample could not be crystallized (with the procedures used).

2.4. Electrochemical measurements

2.4.1. Al corrosion

Samples (solvent–LiX or IL–LiX mixtures) were prepared in the glovebox according to Table 1. The concentrations of the carbonate-based and IL-based mixtures were 1.0 *m* and 0.5 *m*, respectively. The later concentrations (for the IL–LiX mixtures) were selected due to LiX salt solubility limitations. These compositions are comparable to those typically reported in related studies [24,32–35]. CR2032 Al-clad coin-cells were constructed in a dry room (RH <0.1% at 20 °C) with 7/16″ (0.97 cm^2) Al working electrodes, Celgard 3501 separators and Li/Li^+ counter/reference electrodes (FMC Lithium). Cyclic voltammograms (CVs) were performed on a Solartron SI-1287 electrochemical interface by cycling each cell from OCV to 6.0 V (vs. Li/Li^+) for two cycles at a rate of 1 mV s^{-1}. Data was processed with CorrView (v. 2.3) software. Upon completion of the cycles, each electrode was removed from the cell, rinsed with AN, and observed through a Nikon Eclipse LV100 illuminated microscope. Optical photos were taken using the microscope and ACT-1 software (v. 2.63) with 100×, 20× and 5× objectives using brightfield or darkfield illumination.

2.4.2. Electrochemical stability

Ceramic patterned cells were obtained from Pine Research Instrumentation that consist of patterned Pt working and counter electrodes. A reference electrode (Ag/Ag^+) was made by immersing a Ag wire in a 10 mM solution of $AgCF_3SO_3$ (AgTf) in $PY_{14}TFSI$ with a fine glass frit. This reference electrode is reported to be stable to within ±1 mV over a period of 3 weeks with a reference electrode potential of 3.40 V (±5 mV) vs. Li/Li^+ [36–38]. The Pt electrodes were cleaned before each test by cycling in the range ±0.8 V in 0.5 M H_2SO_4 (with a Ag wire immersed as the reference electrode), rinsing with deionized H_2O and EA, and drying in the oven at 120 °C for 1 h. The final scan of this H_2SO_4 cycling was used to calculate the real surface area of the Pt electrode by hydrogen absorption [39]. The surface area was calculated before each test to ensure accuracy, with a typical value of 0.80 cm^2. To determine the electrochemical stability of each IL and IL–LiX mixture, the samples were added to a low-volume voltammetry cell (Pine Research Instrumentation) in the glovebox, along with a clean Pt-patterned cell and the Ag/Ag^+ reference electrode. The samples were cycled (5 mV s^{-1}) three times from OCV (approximately −0.5 V) to 2.4 V and from OCV to −4.0 V by a Biologic VMP3 potentiostat/galvanostat/EIS. Data was processed with EC-Lab (v. 10.21) software. For convenience, all of the data were converted to a Li/Li^+ reference using the potential noted previously. The notation used for cathodic and anodic scans refers to scanning the potential to lower or higher values, respectively.

Table 1
Summary of corrosive(C)/non-corrosive (NC) properties of carbonate- and IL-based electrolytes.

	LiTFSI	LiFSI	$LiPF_6$	LiDFOB
EC/DMC	C	C	NC	NC
EC/EMC	C	C	NC	NC
$PY_{14}TFSI$	NC	C[a]	NC	NC
$PY_{14}DFOB$	NC	NC	NC	NC

[a] Very low corrosive current.

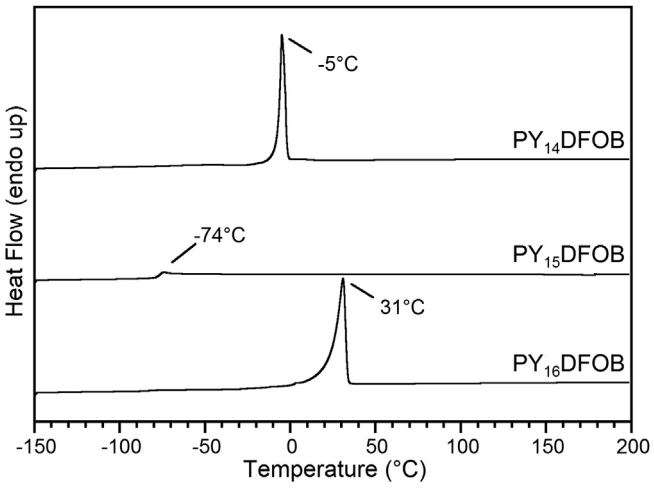

Fig. 1. DSC heating traces (5 °C min^{-1}) of the $PY_{14}DFOB$, $PY_{15}DFOB$ and $PY_{16}DFOB$ ILs.

3. Results and discussion

3.1. Purity evaluation

Purity is a critical criterion for battery electrolytes. NMR spectra were therefore obtained to characterize the ILs. ^{1}H-NMR spectra of the $PY_{1R}DFOB$ ILs (with CD_3CN) were used to determine if any proton-containing impurities were present. A small amount of a

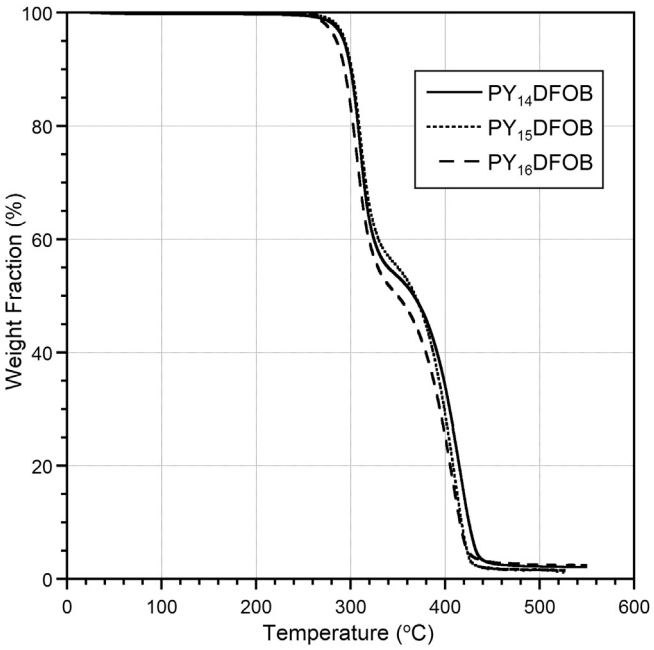

Fig. 2. TGA heating traces (5 °C min^{-1}) of the $PY_{14}DFOB$, $PY_{15}DFOB$ and $PY_{16}DFOB$ ILs.

proton-containing impurity was observed at 4.46 ppm in the $PY_{15}DFOB$ and $PY_{16}DFOB$ ILs, but identification of this impurity was unsuccessful and further attempts to purify the ILs lead to no noticeable decrease in the impurity concentration.

^{11}B NMR spectra were used to analyze the concentration of BF_4^- and BOB^- anions present in the ILs, as the $DFOB^-$ anion is known to disproportionate into these anions (due to thermodynamic equilibrium) [40]. To determine the detection limit of this technique, LiDFOB was dissolved in CD_3CN and spiked with 0.1 mol% $LiBF_4$ and LiBOB. This test confirmed, by integrating the resulting spectra, that levels of $\geq$0.1 mol% BF_4^- and BOB^- could be observed through ^{11}B NMR analysis. Schreiner *et al.* also report the use of this technique with a limit of detection of ~0.05–0.10 mol% [26]. The purity of the ILs (in terms of the anions) was thus determined to be approximately 96.9%, 97.0% and 96.2% for $PY_{14}DFOB$, $PY_{15}DFOB$ and $PY_{16}DFOB$, respectively. Due to the disproportionation reaction, the purity limits of the ILs actually represent the intrinsic equilibrium of the $DFOB^-$ anions with small amounts of BF_4^- and BOB^- anions, which will always be present in these ILs.

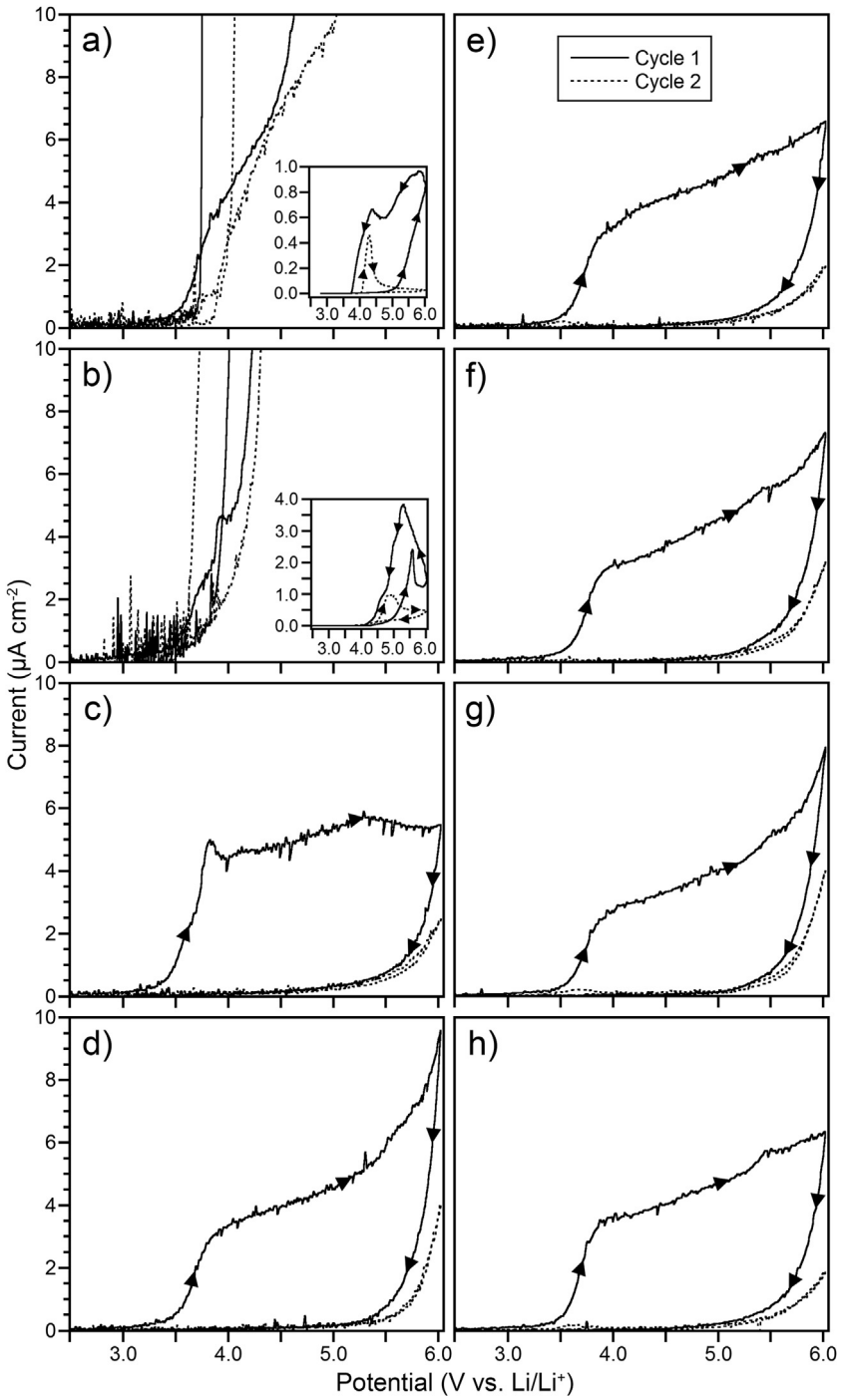

Fig. 3. Cyclic voltammograms (Al working electrode) of (a–d) EC/DMC–LiX and (e–h) $PY_{14}DFOB$–LiX mixtures with (a,e) LiTFSI, (b,f) LiFSI, (c,g) $LiPF_6$ and (d,h) LiDFOB. Full scale plots are shown in the insets (mA cm^{-2} units used for clarity). Scans were performed at 1 mV s^{-1}.

3.2. Thermal measurements

3.2.1. Thermal phase behavior

DSC measurements were conducted to determine the T_m and/or T_g of the ILs (Fig. 1). The $PY_{14}DFOB$ salt initially displayed a T_g at −77 °C. Upon multiple cooling/heating scans below/above the T_g, the sample crystallized into a solid phase with a T_m at −5 °C. For comparison, $PY_{14}BF_4$ has a T_m at 142 °C and $PY_{14}BOB$ does not crystallize, but instead has a T_g at −38 °C [41,42]. The T_m for the $PY_{14}DFOB$ salt is similar to that of $PY_{14}TFSI$ (i.e., −3 °C) [43]. The $PY_{15}DFOB$ salt exhibits a T_g at −74 °C and it was not possible to crystallize the salt with the thermal cycling/annealing conditions used, despite extensive efforts to do so. The $PY_{16}DFOB$ salt, similar to $PY_{14}DFOB$, did not crystallize during the initial cooling scan. Subsequent heating indicated a T_g at −74 °C followed by crystallization (thermal cycling). The resulting crystalline phase has a T_m at 31 °C. Despite the T_m above ambient temperature, the $PY_{16}DFOB$ salt remained a liquid (after melting) at room temperature throughout all of the testing. This salt could only be crystallized upon cycling multiple times at low temperature (crystallization onset at −27 °C) indicating that the nucleation kinetics for the crystalline phase are quite slow.

3.2.2. Thermal stability

Fig. 2 shows the TGA heating traces for the ILs which indicate their approximate decomposition temperature (T_d). The ILs all display a similar two-step decomposition pathway with an onset temperature of about 290 °C. This onset temperature is somewhat higher than that noted for LiDFOB, which also undergoes a multi-step decomposition pathway [29].

3.3. Electrochemical measurements

3.3.1. Al corrosion

In order to be utilized as an additive or in lieu of a primary electrolyte solvent, the ILs must be non-corrosive toward the Al current collector widely used with cathode materials. Mixtures with either common carbonate solvents or ILs and various lithium salts were therefore tested. Current state-of-the-art electrolytes are typically composed of 1 M $LiPF_6$ dissolved in EC/linear carbonate (DMC, EMC or diethyl carbonate (DEC)) in a 3/7 volume ratio, which sufficiently passivates the Al current collector and prevents corrosion through the formation of an AlF_3 interfacial layer [44–46]. Similar mixtures with LiDFOB have also been shown to passivate Al [15,16]. LiTFSI and LiFSI, however, are known to corrode Al in such

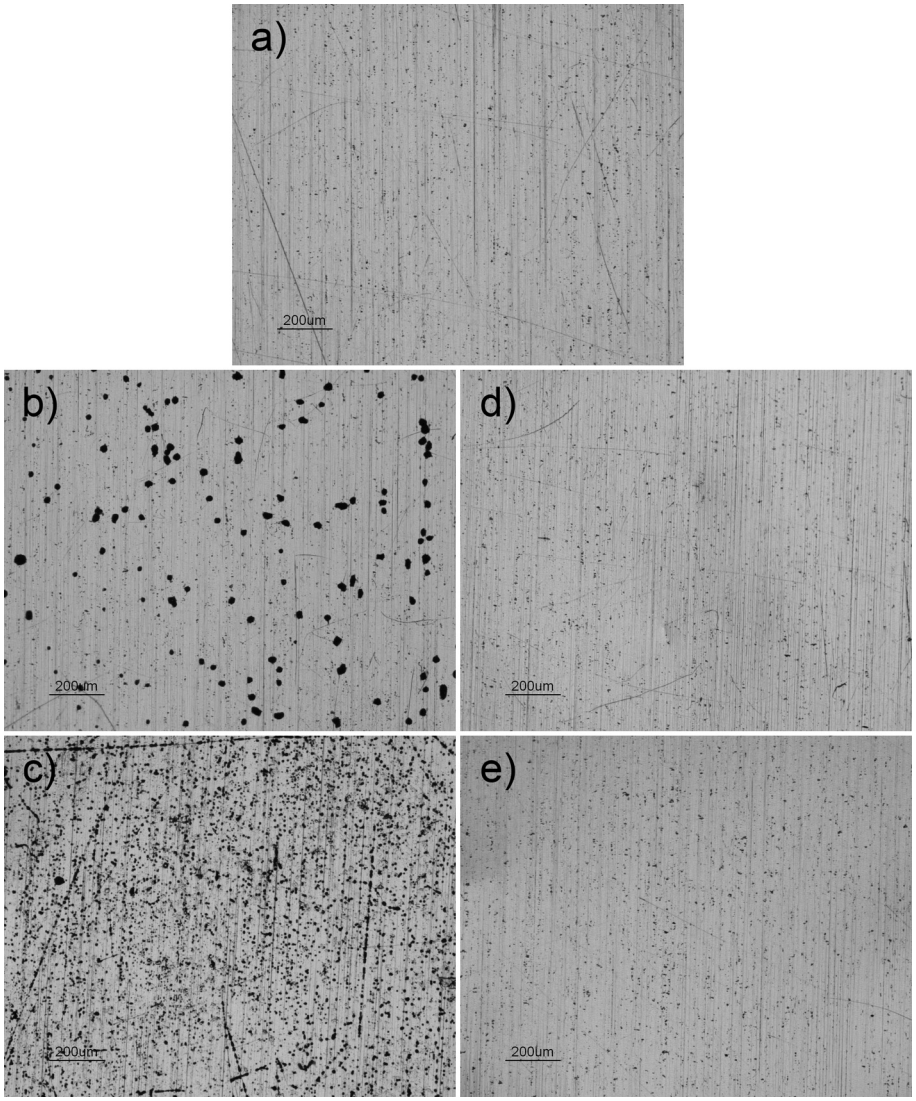

Fig. 4. Surface images of the (a) pristine Al working electrode and Al working electrodes cycled with the (b) EC/DMC–LiTFSI, (c) EC/DMC–LiFSI, (d) $PY_{14}DFOB$–LiTFSI and (e) $PY_{14}DFOB$–LiFSI electrolytes.

solvent mixtures at higher potentials, limiting the usefulness of these salts for high-voltage cells [46–49]. This is evident in Fig. 3, which indicates that a significant corrosive current is present for the carbonate–LiTFSI and carbonate–LiFSI mixtures, but not for the carbonate–$LiPF_6$ and carbonate–LiDFOB mixtures (passivation occurs during the first cycle for the latter salts). It is noteworthy, however, that corrosion only occurs at potentials >4 V for carbonate–LiFSI mixtures, which suggests these electrolytes are suitable for standard (commercial) electrode materials operating at ~3.7 V. Microscope images of the Al electrodes after the CV scans are shown in Figs. 4 and 5. These images confirm that there is extensive pitting-corrosion only for the carbonate–LiTFSI and carbonate–LiFSI mixtures.

ILs such as PY_{1R}TFSI, in contrast to the carbonate solvents, have been reported to prevent Al corrosion, even for mixtures containing LiTFSI [33,50]. The mechanism of corrosion inhibition for ILs is thought to be due to the insolubility of the Al–TFSI or Al–FSI complexes formed from the initial reaction of the salts with the Al at high potential [33]. The complexes effectively passivate the Al surface. The PY_{1R}DFOB ILs also resist Al corrosion, as found for the PY_{1R}TFSI ILs, even when mixed with LiTFSI (Fig. 3). IL–LiFSI mixtures, however, display some unexpected results. PY_{14}TFSI–LiFSI exhibits a CV curve indicative of corrosion, although the current passed is significantly less than for carbonate–LiFSI mixtures (see Fig. S4 in Supplementary data). This suggests that if an $Al(FSI)_3$ complex is formed, it may be marginally soluble in PY_{14}TFSI. The PY_{14}DFOB–LiFSI mixture, on the contrary, shows CV curves indicative of passivation. Thus, PY_{14}DFOB is evidently able to passivate the Al working electrode and prevent corrosion even in circumstances where PY_{14}TFSI cannot. It is unclear which mechanism results in the non-corrosive properties of the PY_{1R}DFOB-based electrolytes—i.e., the decomposition of the $DFOB^-$ anion to form AlF_3 (similar to the PF_6^- anion) or the formation of an $Al(DFOB)_3$ complex (similar to PY_{1R}TFSI). A summary of the results with the different electrolytes is given in Table 1. The complete CVs and corresponding pictures for all of the mixtures tested can be found in Supplementary data.

3.3.2. Electrochemical stability

Voltammograms for each IL (with a Pt working electrode) are shown in Figs. 6 and 7. The oxidation stability limit of the ILs is approximately 5.0 V (vs. Li/Li^+) (Fig. 6). This limit is much higher than might be expected as the anion contains an oxalate group. The stability of the PY_{1R}DFOB ILs is close to the reported 5.2 V anodic stability limit of PY_{14}TFSI, which is attributed to the irreversible oxidization of the $TFSI^-$ anion [32]. The cathodic stability limit, however, is inherently more difficult to determine for these ILs. Surprisingly, the neat PY_{1R}DFOB ILs exhibit partially reversible oxidation/reduction behavior at potentials between 0 and 1 V (Fig. 6). It was initially thought that dissolved gases might be a source of contamination, as it has been reported that a significantly different reduction stability limit is obtained for PY_{14}TFSI with and without dissolved N_2 or O_2 gases [51]. Yet, degassing the ILs (with Ar) at 80 °C for 24 h lead to negligible differences in subsequent voltammetry tests. It was also thought that trace Na^+ cation impurities (if present) might lead to the reversible behavior as Na plating is known to occur around this potential. However, an ICP-MS analysis of the PY_{16}DFOB IL indicated that only ~2 ppm Na was present (see Supplementary data). Further, the elemental analysis of the three ILs found a negligible Br^- anion content which indicates that the ILs are free of NaBr (see Supplementary data). These analyses, and the amount of current passed, suggest instead that this electrochemical behavior is inherent to the PY_{1R}DFOB salts. The origin of this redox behavior is not yet known. It may be that the $DFOB^-$ anions are the reactive species (as this redox behavior is not noted for the PY_{14}TFSI salt—Fig. 7) and that upon reduction, some of the resulting product (from the cathodic scan) diffuses away from the electrode and is thus unavailable for subsequent oxidation (during the anodic scan to higher potential).

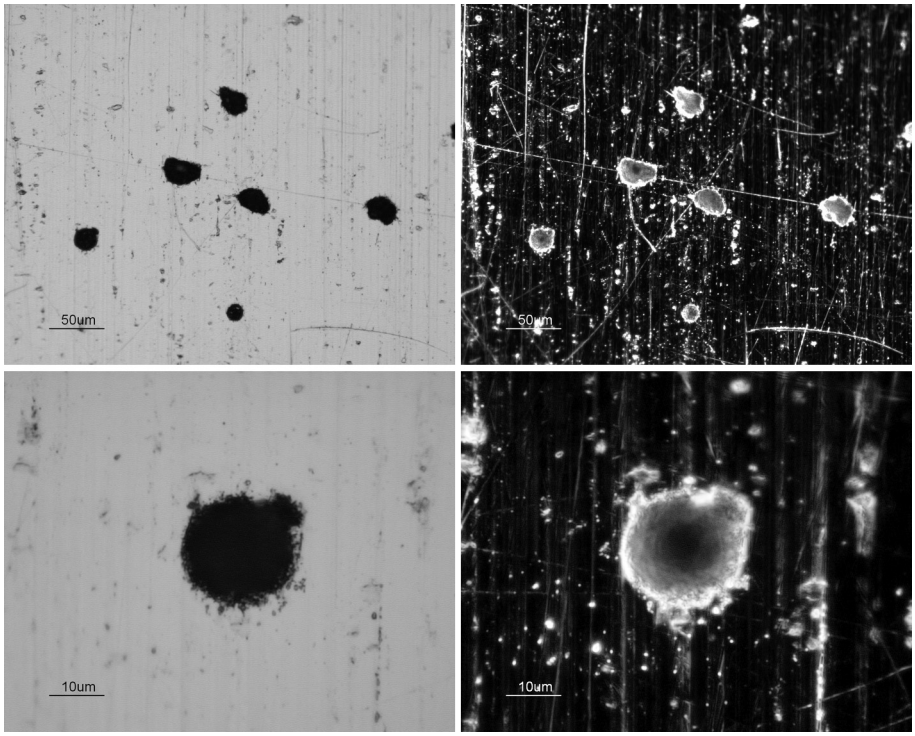

Fig. 5. Brightfield (left) and darkfield (right) images of pitting corrosion on the Al working electrode cycled with the EC/DMC–LiTFSI electrolyte (Fig. 4b) at 20× (top) and 100× (bottom) zoom.

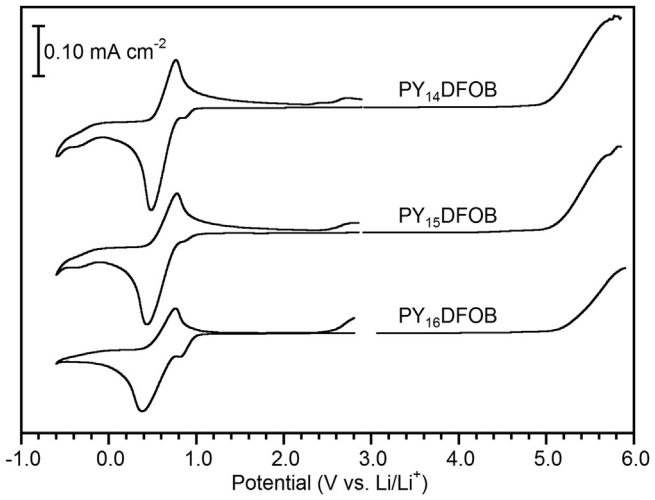

Fig. 6. Voltammograms of the $PY_{14}DFOB$, $PY_{15}DFOB$ and $PY_{16}DFOB$ ILs on a Pt working electrode.

To further examine the electrochemical properties of the ILs, the $PY_{14}DFOB$ and $PY_{14}TFSI$ salts were mixed with either LiDFOB or LiTFSI, as it has been previously noted that the addition of lithium salts can improve the cathodic stability of ILs [52–54]. Interestingly, the addition of the lithium salts to the $PY_{14}DFOB$ IL eliminates the partially reversible redox peaks and consequently enables largely reversible Li/Li^+ plating/stripping (with a coulombic efficiency of 90% or greater after the initial cycle), similar to that found for the $PY_{14}TFSI$ ILs (Fig. 7). It is notable that the voltammograms displayed multiple peaks, including peaks above 1.0 V vs. Li/Li^+ during the anodic scans. These are due to Pt_xLi alloy formation, as well as Li plating. During the cathodic scan, the Pt_xLi alloys are formed with subsequent Li plated on top of the alloys. In the reverse (anodic) scan, the plated Li metal is oxidized first, then the Pt_xLi alloys are oxidized as multiple peaks, depending upon which alloy was formed [55,56]. A comparison of the $PY_{14}TFSI$ and $PY_{14}DFOB$ voltammograms indicates that the cation is likely not responsible for the (partially) reversible behavior at low potentials, given that these ILs share a common cation. This suggests that the partially reversible redox peak for the $PY_{1R}DFOB$ ILs (in the absence of Li^+ cations) may instead be attributed to chemistry associated with the $DFOB^-$ anions.

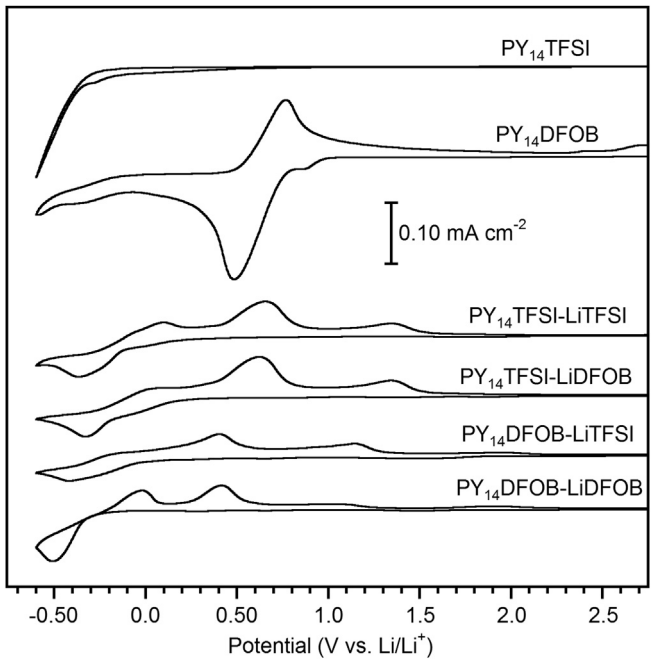

Fig. 7. Voltammograms of the ILs and IL–LiX electrolytes on a Pt working electrode.

4. Conclusions

$PY_{1R}DFOB$ ILs are difficult to purify due to the presence of an equilibrium concentration of BF_4^- and BOB^- anions formed from the thermodynamic disproportionation reaction of the $DFOB^-$ anions. A DSC analysis of the ILs indicated T_m values of −5 °C and 31 °C, respectively, for the $PY_{14}DFOB$ and $PY_{16}DFOB$ salts, while the $PY_{15}DFOB$ salt did not crystallize (instead a T_g at −74 °C was noted). All three ILs possess a high thermal stability, displaying a two-step thermal decomposition pathway with an onset temperature of ~290 °C for each IL. Similar to $TFSI^-$-based IL electrolytes, the $PY_{1R}DFOB$–LiX mixtures do not corrode Al, even in mixtures with LiTFSI and LiFSI (salts known to corrode Al in carbonate-based electrolytes at higher potentials). Electrochemical stability testing of the neat $PY_{1R}DFOB$ ILs suggests that they are stable up to 5.0 V (vs. Li/Li^+). The addition of lithium salts (i.e., LiDFOB or LiTFSI) results in an improvement in the cathodic stability of the mixtures (relative to the neat ILs) with reversible Li/Li^+ plating/stripping observed. The thermal and electrochemical properties of the $PY_{1R}DFOB$ ILs suggest they are potentially well-suited for battery electrolyte applications.

Acknowledgments

This work was fully funded by the U.S. DOE BATT Program (contract number DE-AC02-05-CH11231). The authors would like to thank Kim Hutchison (Department of Soil Science, North Carolina State University) for the ICP-MS analysis and Dr. Hanna Gracz (Biomolecular NMR Facility, North Carolina State University) for the ^{11}B NMR analysis. J.L.A. would like to thank the SMART Scholarship Program and the American Society for Engineering Education (ASEE) for the award of a SMART Graduate Research Fellowship.

Appendix A. Supplementary data

Supplementary data associated with this article can be found in the online version, at http://dx.doi.org/10.1016/j.jpowsour.2013.02.086.

References

[1] L.E. Ouatani, R. Dedryvere, C. Siret, P. Biensan, S. Reynaud, P. Iratcabal, D. Gonbeau, J. Electrochem. Soc. 156 (2009) A103.
[2] L.E. Ouatani, R. Dedryvere, C. Siret, P. Biensan, D. Gonbeau, J. Electrochem. Soc. 156 (2009) A468.
[3] H.-C. Wu, C.-Y. Su, D.-T. Shieh, M.-H. Yang, N.-L. Wu, Electrochem. Solid-State Lett. 9 (2006) A537.
[4] Y. An, P. Zuo, C. Du, Y. Ma, X. Cheng, J. Lin, G. Yin, RSC Adv. 2 (2012) 4097.
[5] S. Dalavi, M. Xu, B. Knight, B.L. Lucht, Electrochem. Solid-State Lett. 15 (2011) A28.
[6] C. Taubert, M. Fleischhammer, M. Wohlfahrt-Mehrens, U. Wietelmann, T. Buhrmester, J. Electrochem. Soc. 157 (2010) A721.
[7] M. Hu, J. Wei, L. Xing, Z. Zhou, J. Appl. Electrochem. 42 (2012) 291.
[8] J. Liu, Z. Chen, S. Busking, K. Amine, Electrochem. Commun. 9 (2007) 475.
[9] J. Li, K. Xie, Y. Lai, Z. Zhang, F. Li, X. Hao, X. Chen, Y. Liu, J. Power Sources 195 (2010) 5344.
[10] M.H. Fu, K.L. Huang, S.Q. Liu, J.S. Liu, Y.K. Li, J. Power Sources 195 (2010) 862.
[11] Z. Chen, J. Liu, K. Amine, Electrochem. Solid-State Lett. 10 (2007) A45.
[12] A. Xiao, L. Yang, B.L. Lucht, S.-H. Kang, D.P. Abraham, J. Electrochem. Soc. 156 (2009) A318.
[13] S.S. Zhang, J. Power Sources 163 (2007) 713.
[14] S.-H. Kang, D.P. Abraham, A. Xiao, B.L. Lucht, J. Power Sources 175 (2008) 526.

[15] A. Lex-Balducci, R. Schmitz, R.W. Schmitz, R.A. Muller, M. Amereller, D. Moosbauer, H. Gores, M. Winter, ECS Trans. 25 (2010) 13.
[16] S. Zugmann, D. Moosbauer, M. Amereller, C. Schreiner, F. Wudy, R. Schmitz, R. Schmitz, P. Isken, C. Dippel, R. Muller, M. Kunze, A. Lex-Balducci, M. Winter, H.J. Gores, J. Power Sources 196 (2011) 1417.
[17] D. MacFarlane, The Handbook of Ionic Liquids, Electrochemistry, Wiley Interscience, New York, NY, 2009.
[18] H. Sakaebe, H. Matsumoto, in: H. Ohno (Ed.), Electrochemical Aspects of Ionic Liquids, Wiley, Hoboken, NJ, 2011.
[19] A. Lex-Balducci, W.A. Henderson, S. Passerini, in: Y. Yuan, H. Liu, J. Zhang (Eds.), Lithium Ion Batteries: Advanced Materials and Technologies, CRC Press, Boca Raton, FL, 2011.
[20] H. Zheng, K. Jiang, T. Abe, Z. Ogumi, Carbon 44 (2006) 203.
[21] Y. Katayama, M. Yukumoto, T. Miura, Electrochem. Solid-State Lett. 6 (2003) A96.
[22] T. Sugimoto, Y. Atsumi, M. Kikuta, E. Ishiko, M. Kono, M. Ishikawa, J. Power Sources 189 (2009) 802.
[23] T. Sugimoto, M. Kikuta, E. Ishiko, M. Kono, M. Ishikawa, J. Power Sources 183 (2008) 436.
[24] A.P. Lewandowski, A.F. Hollenkamp, S.W. Donne, A.S. Best, J. Power Sources 195 (2010) 2029.
[25] M. Nadherna, J. Reiter, J. Moskon, R. Dominko, J. Power Sources 196 (2011) 7700.
[26] C. Schreiner, M. Amereller, H.J. Gores, Chem.—Eur. J. 15 (2009) 2270.
[27] H. Sakaebe, H. Matsumoto, Electrochem. Commun. 5 (2003) 594.
[28] H. Matsumoto, H. Sakaebe, K. Tatsumi, M. Kikuta, E. Ishiko, M. Kono, J. Power Sources 160 (2006) 1308.
[29] J.L. Allen, S.D. Han, P.D. Boyle, W.A. Henderson, J. Power Sources 196 (2011) 9737.
[30] J.L. Allen, P.D. Boyle, W.A. Henderson, Acta Crystallogr. E67 (2011) m678.
[31] E.T. Fox, J.E.F. Weaver, W.A. Henderson, J. Phys. Chem. C 116 (2012) 5270.
[32] J. Jin, H.H. Li, J.P. Wei, X.K. Bian, Z. Zhou, J. Yan, Electrochem. Commun. 11 (2009) 1500.
[33] R.-S. Kuhnel, M. Lubke, M. Winter, S. Passerini, A. Balducci, J. Power Sources 214 (2012) 178.
[34] G.B. Appetecchi, M. Montanino, A. Balducci, S.F. Lux, M. Winter, S. Passerini, J. Power Sources 192 (2009) 599.
[35] J. Reiter, M. Nadherna, Electrochim. Acta 71 (2012) 22.
[36] G.A. Snook, A.S. Best, A.G. Pandolfo, A.F. Hollenkamp, Electrochem. Commun. 8 (2006) 1405.
[37] E.I. Rogers, D.S. Silvester, S.E.W. Jones, L. Aldous, C. Hardacre, A.J. Russel, S.G. Davies, R.G. Compton, J. Phys. Chem. C 111 (2007) 13957.
[38] Q. Zhou, W.A. Henderson, G.B. Appetecchi, M. Montanino, S. Passerini, J. Phys. Chem. B 112 (2008) 13577.
[39] J.M.D. Rodriguez, J.A.H. Melian, J. Chem. Educ. 77 (2000) 1195.
[40] L. Zhou, W. Li, M. Xu, B. Lucht, Electrochem. Solid-State Lett. 14 (2011) A161.
[41] S. Forsyth, J. Golding, D.R. MacFarlane, M. Forsyth, Electrochim. Acta 46 (2001) 1753.
[42] W. Xu, L.-M. Wang, R.A. Nieman, A. Angell, J. Phys. Chem. B 107 (2003) 11749.
[43] W.A. Henderson, S. Passerini, Chem. Mater. 16 (2004) 2881.
[44] S.S. Zhang, T.R. Jow, J. Power Sources 109 (2002) 458.
[45] J.W. Braithwaite, A. Gonzales, G. Nagasubramanian, S.J. Lucero, D.E. Peebles, J.A. Ohlhausen, W.R. Cieslak, J. Electrochem. Soc. 146 (1999) 448.
[46] H. Yang, K. Kwon, T.M. Devine, J.W. Evans, J. Electrochem. Soc. 147 (2000) 4399.
[47] M. Morita, T. Shibata, N. Yoshimoto, M. Ishikawa, J. Power Sources 119–121 (2003) 784.
[48] L.J. Krause, W. Lamanna, J. Summerfield, M. Engle, G. Korba, R. Loch, R. Atanasoski, J. Power Sources 68 (1997) 320.
[49] A. Abouimrane, J. Ding, I.J. Davidson, J. Power Sources 189 (2009) 693.
[50] B. Garcia, M. Armand, J. Power Sources 132 (2004) 206.
[51] S. Randstrom, G.B. Appetecchi, C. Lagergren, C. Moreno, S. Passerini, Electrochim. Acta 53 (2007) 1837.
[52] G.B. Appetecchi, S. Scaccia, C. Tizzani, F. Alessandrini, S. Passerini, J. Electrochem. Soc. 153 (2006) A1685.
[53] H. Matsumoto, H. Kageyama, Y. Miyazaki, Electrochemistry 71 (2003) 1058.
[54] Y. Katayama, T. Morita, M. Yamagata, T. Miura, Electrochemistry 71 (2003) 1033.
[55] D. Baril, Y. Chabre, Electrochem. Solid-State Lett. 4 (2001) E21.
[56] A.N. Dey, J. Electrochem. Soc. 118 (1971) 1547.